Journal of Power Sources 196 (2011) 7450–7457

Contents lists available at ScienceDirect

Journal of Power Sources

journal homepage: www.elsevier.com/locate/jpowsour

Dodecylamine-modified carbon supports for cathode in proton exchange membrane fuel cells

Juei Dong Lu, Ming-Chang Yang*

Department of Chemical Engineering, National Cheng Kung University, Tainan 701, Taiwan

ARTICLE INFO

Article history:
Received 4 March 2011
Received in revised form 24 April 2011
Accepted 26 April 2011
Available online 30 April 2011

Keywords:
Proton exchange membrane fuel cell
Catalyst
Cathode
Carbon support
Chemical modification

ABSTRACT

In this investigation, hydrophobic dodecylamine-modified carbon supports are prepared for proton exchange membrane fuel cells by organic synthesis. Well-dispersed Pt–Ru nanoparticles, with a narrow size distribution, are then deposited on the dodecylamine-modified carbon supports by methanol reduction to serve as cathodic catalysts. These dodecylamine-modified catalysts are separately mixed with either a commercial catalyst or unmodified catalyst to provide hydrophobic channels to convey the reaction gas to the active sites in the catalyst layer. The best cathode composite catalyst, containing 20–40 wt% of modified-catalyst, gives approximate 30% increase in the maximum power density, comparing to E-TEK catalyst (125 mW cm^{-2}). The increase in the maximum power density is attributed to higher activity and lower resistance. This result is discussed in the context of AC-impedance and proton conductivity analysis.

1. Introduction

Proton exchange membrane fuel cells (PEMFCs) have been the subject of much interest due to their potential as power sources for stationary and vehicular applications. With the goal of attaining a high power level and reducing the amount of noble metal used, one strategy has been to increase catalytic activity in the electrode by increasing the density of active sites by ensuring that the metal nanoparticles are highly dispersed. To achieve this, surfactants are often used as stabilizers to synthesize well dispersed metal nanoparticles, with a narrow-size distribution, on carbon supports [1,2]. Although well dispersed metal nanoparticles can be formed using surfactants, the removal of the surfactants from the nanoparticle surface is an important issue. In addition to the effects resulting from the use of surfactant, the pore structure and the functional group chemistry affect the dispersion of metal nanoparticles. Therefore, metal dispersion has also been investigated by modifying the surface of the carbon supports by the introduction of desired functional groups [3,4,13].

In order to achieve a high utilization of the catalyst, other factors apart from the dispersion of metal nanoparticles, such as the structure and hydrophobicity of the catalytic layer are important. Fischer et al. [5] reported that the addition of pore-forming additives in the catalytic layer improved catalyst utilization and cell performance. The fine pore system, when made without pore-forming additives, seemed to be almost completely filled with water at high current densities. Wilson and Gottesfeld [6] reported that the addition of Teflon can increase the diffusivity of gases as it provides hydrophobicity to an open pore, thereby helping to avoid clogging with water. But loading the catalyst layer with PTFE lowers the utilization of the catalyst in completely dry or Teflon-coated active sites. One solution to the above problem has been to load PTFE on carbon supports without metal nanoparticles, forming a PTFE-C conjugate, and then to add this into the catalytic ink for MEA preparation [7]. Because the PTFE-C forms dry pores in the catalytic layer, it was able to enhance the transportation of the gas and water. However, the thickness of the catalytic layer increased with the content of PTFE-C in catalyst layer.

In this study, dodecylamine was introduced on the surface of the carbon supports using an organic synthetic method. The dodecylamine chains on the carbon surface were able to act as the capping agent for the well dispersed metal nanoparticles, as shown in Fig. 1, which were obtained after the reduction of metal salt by methanol. It is believed that catalytic layer with the dodecylamine-modified catalyst contained within hydrophobic channels is beneficial to gas diffusion. In contrast, the unmodified catalyst shows more hydrophilic micro-pores that serve as water-flow paths. In order to satisfy the requirements of the transportation of both, gases and water, a composite catalyst layer comprising dodecylamine-modified catalyst and unmodified catalyst was prepared to form ducts in the catalytic layer to permit the transit of gases and water.

* Corresponding author. Tel.: +866 6 275 7575x62666; fax: +886 6 234 4496.
E-mail address: mcyang@mail.ncku.edu.tw (M.-C. Yang).

0378-7753/$ – see front matter © 2011 Elsevier B.V. All rights reserved.
doi:10.1016/j.jpowsour.2011.04.055

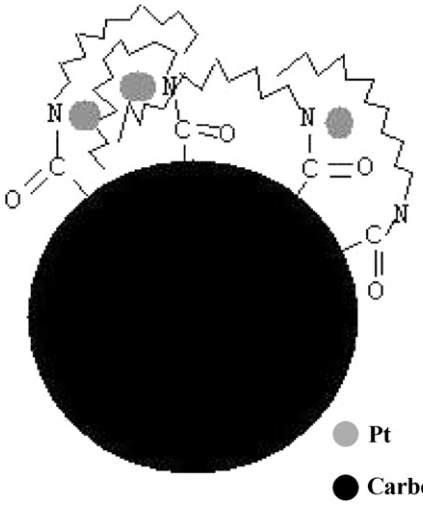

Fig. 1. Schematics of Pt nanoparticles on a dodecylamine-modified carbon support.

2. Experimental

2.1. Surface modification of carbon

In order to clean the carbon surface, Vulcan XC-72 carbon, termed carbon (raw), was pretreated in concentrated HCl (37% Scharlau) at 70 °C for 12 h. The purified carbon was initially modified according to a published method that introduced an amide bond [3]. In brief, the purified carbon was stirred in concentrated HNO_3 (65% Scharlau) at 70 °C for 5 h to form a carboxyl group. Then the carboxyl-functionalized carbon was chlorinated by refluxing in $SOCl_2$. After removal of the residual $SOCl_2$ (Aldrich 98%) by distillation, the acyl chloride-functionalized carbon was reacted with excess dodecylamine (ACROS) in toluene to obtain the final desired carbon (modified).

2.2. Electrocatalyst preparation

Pt–Ru nanoparticles were deposited on the carbon supports by impregnation of the platinum and ruthenium salts followed by methanol reduction [8]. H_2PtCl_6 (ACROS), $RuCl_3$ (Strem) and the carbon supports were mixed in D.I. water for 4 h. The concentration of H_2PtCl_6 and $RuCl_3$ was 0.0356 M and 0.0364 M in the mixture, respectively. Subsequently, Pt–Ru particles were deposited by the addition of methanol (water:methanol = 2:1) in the mixture and then cooled, filtered, and washed with D.I. water several times. After drying, 20 wt% Pt–Ru nanoparticles on carbon was obtained. The resulting catalysts with unmodified and modified carbons were termed Pt–Ru/C (raw) and Pt–Ru/C (modified), respectively.

2.3. Preparation of membrane electrode assembly

To prepare the cathodic catalytic layers, catalytic ink, comprising the catalysts and an aqueous Nafion® solution (5%, Aldrich) at a carbon/dry Nafion ratio of 7:3 and a Nafion solution/water ratio of 1:1, was prepared. The catalytic ink was quantitatively deposited, by brushing, on one side of the wet-proofed carbon papers (TGPH-060, Toray) with a Pt loading of 0.8 mg cm^{-2}. Commercial Pt–Ru/C (E-TEK, 20 wt% Pt–Ru), Pt–Ru/C (raw), Pt–Ru/C (modified) and composite catalysts were used to make the cathodes. Pt–Ru/C (raw) and E-TEK catalyst were separately mixed with Pt–Ru/C (modified) catalyst at various ratios as composite catalysts (raw) and composite catalysts (E-TEK), respectively. Similarly, the anode used in the experiment was composed of wet-proofed carbon paper and the coated Pt–Ru/C (raw) catalyst. The electrodes, which were dried at room temperature for MEA formation, had exposed areas measuring 2.5 × 2.5 cm^2.

A platinum film (1.0 × 2.5 cm^2) was deposited on a Nafion 117 membrane (Dupont) as a pseudo-reference electrode, according to a previous report [8]. A three-electrode membrane electrode assembly (3E-MEA) was made by hot pressing the prepared anode and cathode on both side of the reference-deposited membrane at 135 °C at a pressure of 30 kg cm^{-2} for 1.5 min. This assembly

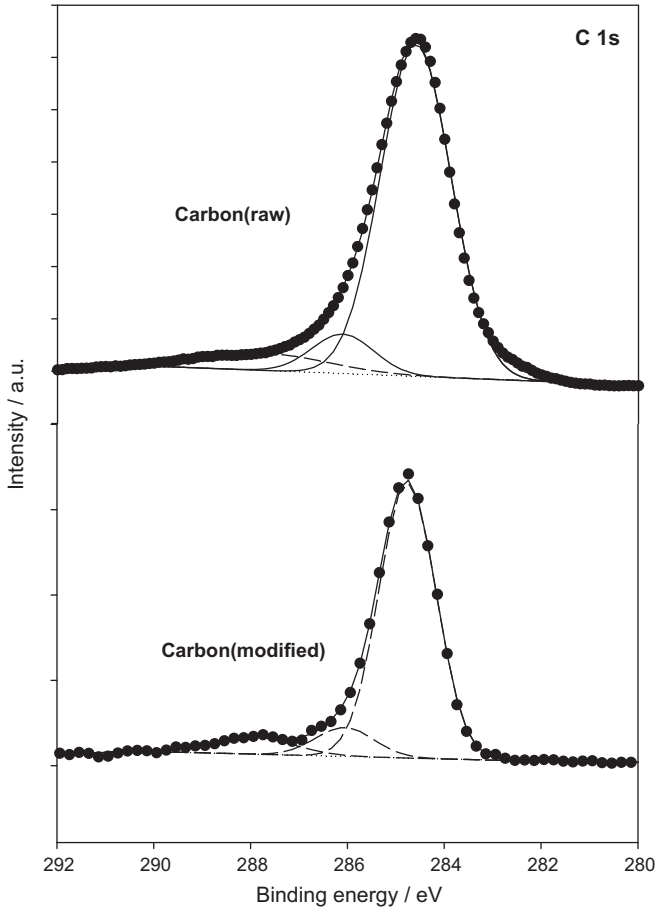

Fig. 2. The XPS spectra of C 1s region for carbon (●, raw data; —, fitting data; ---, deconvoluted data).

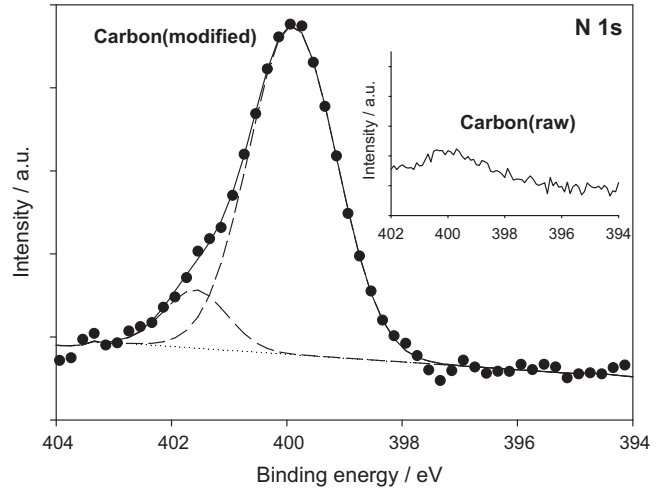

Fig. 3. The XPS spectra of N 1s region for carbon (modified) (●, raw data; —, fitting data; --, deconvoluted data). The insert shows the N 1s line for carbon (raw).

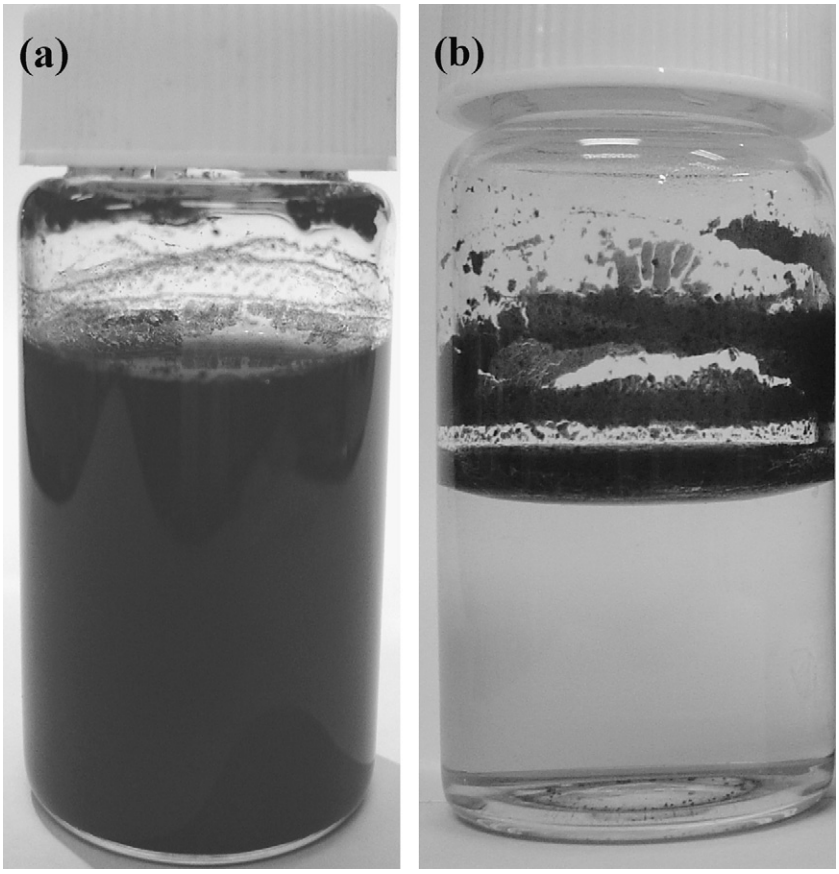

Fig. 4. Photographs of (a) carbon (raw) and (b) carbon (modified) dispersed in water.

afforded the analysis of the individual electrodes during discharging and electrochemical impedance analysis.

2.4. Physical characteristics

The morphological characteristics of the catalysts were examined using transmission electron microscopy (TEM, H7500, Hitachi), and X-ray diffractometry (XRD, D/MAX, RIGAKU) analysis that was carried out using a Cu-K_α source at room temperature. The average particle size was calculated from Pt (1 1 1) peak with the Debye-Scherrer equation fitted by a Gaussian function. The hydrophobic property was evaluated by measuring the contact angle of water droplet on the surface of a carbon disk, made by applying a pressure of 40 kg cm^{-2} to 0.127 g cm^{-2} of carbon powder. X-ray photoelectron spectroscopy (XPS) was carried out using a VG Scientific ESCALAB 210 electron spectrometer with Mg-K_α radiation under a vacuum of 2×10^{-8} Pa. Narrow scan photoelectron spectra were recorded in the C 1s and N 1s regions and analyzed by deconvolution.

2.5. Electrochemical measurements of single cells

The 3E-MEA was installed as a single cell. The reaction gases (hydrogen/oxygen) were fed into the cell, which was held at 70 °C, at a flow rate of 100 ml min^{-1} while the anode and cathode gases were maintained at 95 °C and 60 °C, respectively. The polarization curves of the cell at steady state were collected using an electronic load (model 63010 from Chroma), while the anode and cathode polarization curves were simultaneously measured against a pseudo-reference electrode using a multimeter (model 803 from Prova). The cathodic electrochemical impedance spectrum was analyzed at a bias of either 0.52 or 0.8 V referred to the pseudo-reference electrode at frequencies ranging from 5 kHz to 10 mHz. The amplitude of the ac signal was 10 mV. Prior to each impedance spectrum, the cell was controlled at either 0.52 or 0.8 V for 300 s.

3. Result and discussion

3.1. Physical properties of modified carbon

The surface states of the carbon (raw) and carbon (modified) were elucidated with XPS, as shown in Figs. 2 and 3 for C 1s and N

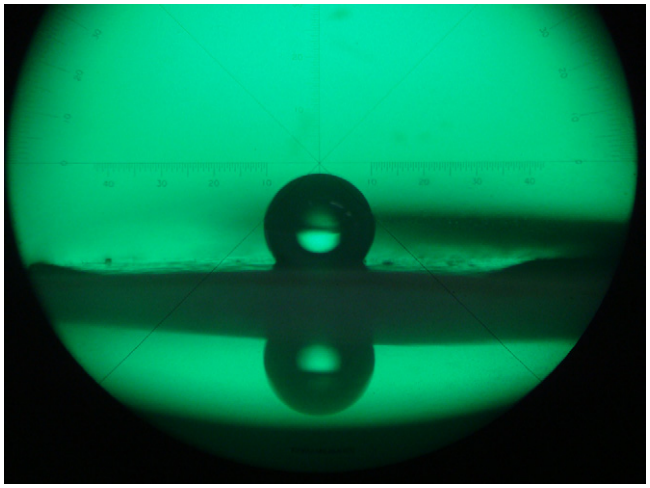

Fig. 5. A droplet of water on a carbon (modified) disk.

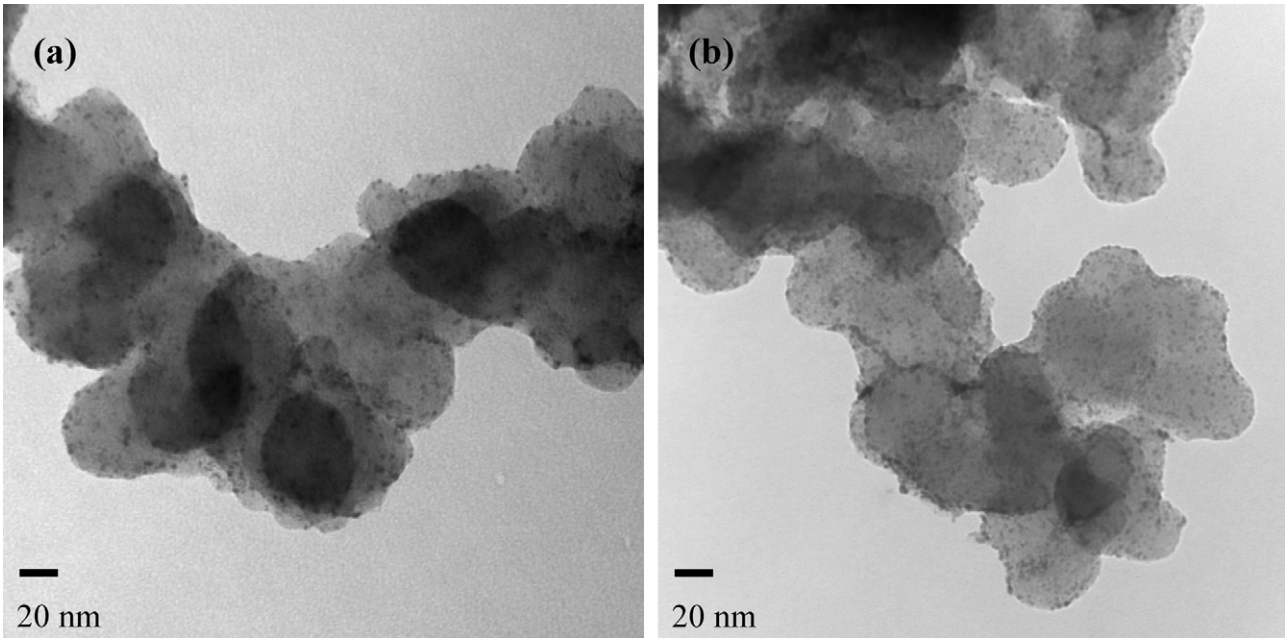

Fig. 6. TEM image of (a) Pt–Ru/C (raw) and (b) Pt–Ru/C (modified).

1s, respectively. The C 1s spectra show strong peaks at 284.6 eV for graphitic carbon in both carbon samples. For both carbon, the simulated curves for C 1s suggest the presence of –C=O with the peak at 286 eV and carbonyl carbons, such as –COOH and –COOR, with the peak at 288 eV [12,13]. Fig. 3 is the XPS for the N 1s peaks in the range 398–402 eV [13–16]. Deconvolution of the N 1s spectra of carbon (modified) gave two peaks at 399.9 and 401.5 eV, which represent the electrostatic interaction of N with a nanoparticle surface [14,16]. The peak at 401.5 eV also can be considered as the quaternary ammonium moieties [15]. However, no peak for nitrogen species appears in the N 1s spectrum of carbon (raw), as shown in the insert of Fig. 3.

Carbon (raw) and carbon (modified) were separately dispersed in water using a vortex mixer. The carbon (raw) dispersed in water

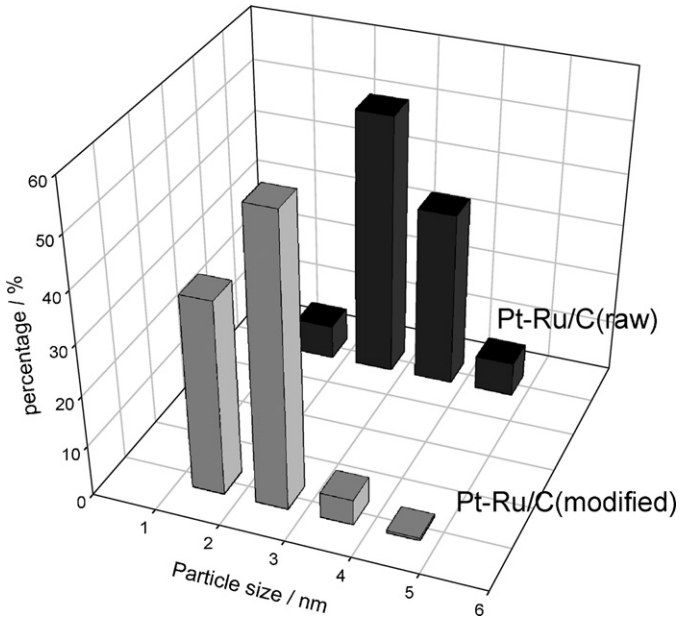

Fig. 7. Size distributions of Pt–Ru nanoparticles in Pt–Ru/C (raw) and Pt–Ru/C (modified), evaluated from TEM images.

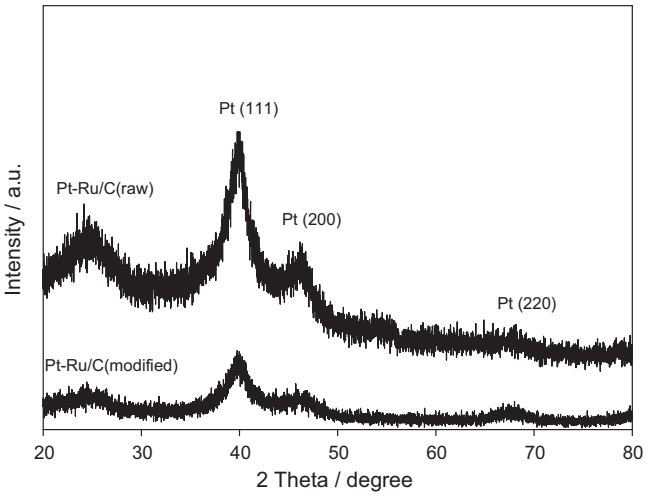

Fig. 8. XRD spectra of Pt–Ru/C (raw) and Pt–Ru/C (modified).

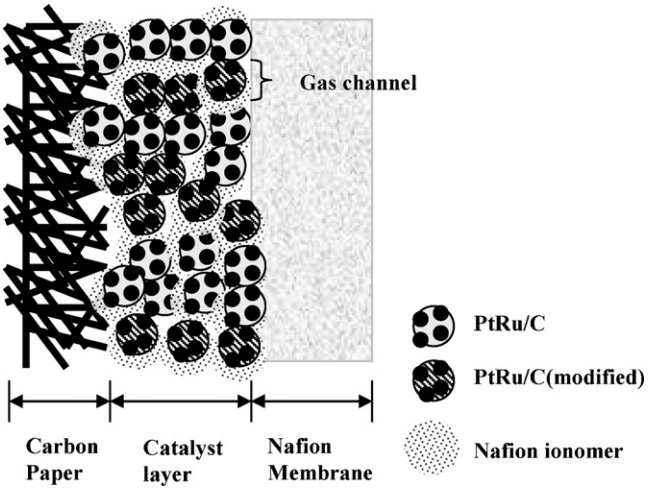

Fig. 9. Cross-sectional schematics of the cathode.

after stirring, as shown in Fig. 4a. In contrast, the carbon (modified) continued to float, as shown in Fig. 4b, demonstrating the hydrophobicity of the material formed. Fig. 5 shows the image of a water droplet on the surface of a carbon chip made by pressuring 0.127 g cm^{-2} of carbon (modified) with a pressure of 40 kg cm^{-2}. The contact angle measurement was made by fitting a tangent to the point where the water surface touched the solid surface. The contact angle (128°) on the surface of the carbon disk implied that it retained the desired hydrophobic behavior of the carbon powders. However, it was difficult to determine the surface contact angle for carbon (raw), due to surface penetration of water droplets; thus, it was obvious that carbon (modified) was more hydrophobic than carbon (raw).

3.2. Characterization of electrocatalysts

Fig. 6a and b shows the typical TEM images of Pt–Ru/C (modified) and Pt–Ru/C (raw), respectively, with the 2–4 nm Pt–Ru nanoparticles being well dispersed. Detailed size distributions, derived from the images are presented in Fig. 7. The average grain sizes were also calculated from the Pt (1 1 1) peaks of the XRD data, presented in Fig. 8, using the Debye-Scherrer equation. The Pt–Ru contents were evaluated by TGA. Detailed catalytic characteristics are listed in Table 1. The average diameters of the Pt–Ru nanoparticles on Pt–Ru/C (modified) and Pt–Ru/C (raw) were determined as 2.2 nm and 2.9 nm, respectively, from TEM measurements, and the corresponding average grain sizes were determined as 3.3 nm and 3.7 nm from XRD measurements. The Pt–Ru/C (modified) shows smaller Pt–Ru nanoparticles on the carbon surface. Two plausible explanations for this are: (i) that the nitric acid oxidation produced dense functional groups on the surface of the carbon supports and that these functional groups supplied enough sites for metal ions and (ii) that the dodecylamine chains on the surface of the carbon supports acted as a capping agent and thus prevented Pt–Ru nanoparticle aggregation. Irrespective of the mechanism, it was apparent that small Pt–Ru nanoparticles were synthesized in situ on the modified carbon supports via methanol reduction of ionic Pt–Ru in solution.

3.3. Optimization of composition of catalyst on cathode

A schematic cross section of a cathode, consisting of Pt–Ru/C (modified), Pt–Ru/C and Nafion ionomer, is shown in Fig. 9. The catalyst of Pt–Ru/C is either Pt–Ru/C (raw) or E-TEK. Uchida et al. [7] reported that the reaction gas could be transported to the catalyst through ducts made of PTFE-C that would function simultaneously as a conduit for the removal of product water. In our MEA we believe that, in addition to the electrochemical activity, the hydrophobic Pt–Ru/C (modified) functioned as the duct-making material to facilitate the supply of the reaction gases to the reaction sites in catalyst layer.

Fig. 10a shows the cell performance with various mass fractions of Pt–Ru/C (modified) in composite catalysts (E-TEK) on the cathodes. The optimum composition with the highest maximum power density (i.e. about 162 mW cm^{-2}) was 20–40 wt% Pt–Ru/C (modified) in the composite catalysts (E-TEK). This result showed an approximate 30% increase in the maximum power density, compared to the maximum power density of 125 mW cm^{-2} with E-TEK catalysts (0 wt% Pt–Ru/C (modified)). Although no mass transfer limitation was observed in the polarization curves, the cathode without Pt–Ru/C (modified) catalyst showed a higher potential decay with current increase in high current region than that with 20–40 wt% Pt–Ru/C (modified). As the mass fraction of the Pt–Ru/C (modified) increased from 60 to 100 wt%, the cell performance in the high current region degraded significantly. Fig. 10b shows the individual polarization curves with various mass fractions of Pt–Ru/C (modified) in composite catalysts (E-TEK) on the cathodes. The anodic polarization curves were independent of the composition of cathode, and the cathode polarization curves were close to the cell polarization curves. The variation, due to different compositions of cathode, in cell resistance eventually was the variation in cathode overall resistance.

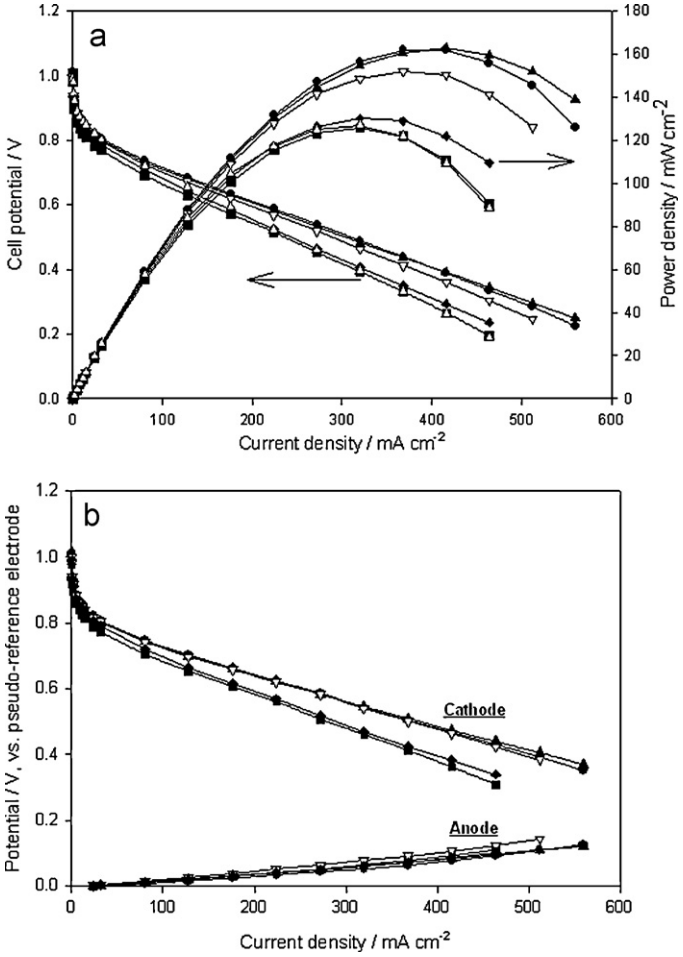

Fig. 10. (a) Cell performances and (b) individual polarization curves with 0 (■), 20 (▲), 40 (●), 60 (▽), 80 (♦) and 100 wt% (△) Pt–Ru/C (modified) in cathode composite catalysts (E-TEK). All of the anode electrode used Pt–Ru/C (raw) as catalysts. The Pt loading for anode and cathode were 0.8 mg cm^{-2}.

In this report, the polarization data of the cathodes were analyzed with the semi-empirical equation proposed by Srinivasan et al. [9]

$$E = E^{o} - b \log i - iR \quad (1)$$

and

$$E^{o} = E_r - b \log i_0 \quad (2)$$

where b, R, E_r and i_0 are Tafel slope, overall resistance, reversible potential and the exchange current for the oxygen reduction reaction (ORR) which is the rate determining step in a PEMFC. The overall resistance includes electrolyte (proton), electrode (electron) and mass transfer resistances. Fig. 11 shows the Tafel slope and the overall resistance vs. the mass fraction of Pt–Ru/C (modified) on the cathode. The Tafel slope and the overall resistance were calculated from cathode polarization curve fitted by Eq. (1). It is noted that Tafel slope decreased slightly with an increase in the mass fraction of the Pt–Ru/C (modified). In a fuel cell system, a lower Tafel slope means a smaller potential dependence on current, resulting smaller charge transfer resistance, which dominates

Table 1
Characteristics of Pt–Ru catalysts on various types of carbon supports.

Type of catalyst	Pt–Ru content from TGA (wt%)[a]	Atomic ratio of Pt/Ru[b] from EDX	Grain size from XRD (nm)	Particle size from TEM (nm)
Pt–Ru/C (modified)	20.4	0.94	3.3	2.2
Pt–Ru/C (raw)	21.4	1.21	3.7	2.9
E-TEK	22.2	0.97	3.6	3.2

[a] Nominal Pt–Ru content = 20 wt%.
[b] Nominal atomic ratio of Pt/Ru = 1.

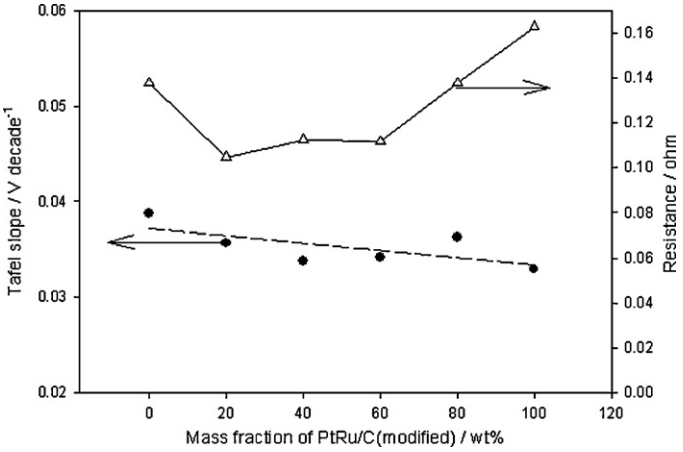

Fig. 11. Tafel slope and resistance vs. the mass fraction of Pt–Ru/C (modified) catalyst in composited catalyst (E-TEK) on the cathode.

the overall resistance at low current density. Therefore, the lower Tafel slope with composite catalysts (E-TEK) gave lower charge transfer resistance that will be also discussed in electrochemical impedance spectrum later. Fig. 11 also shows that the mass fraction of Pt–Ru/C (modified) in the composite catalysts (E-TEK) in the range 20–40 wt% gave lower overall resistance.

The Nyquist plots from electrochemical impedance analysis for the cathode with E-TEK catalysts and 40 wt% composite catalysts (E-TEK) are shown in Fig. 12. There is only a single impedance arc for each spectrum. This single semicircle loop, often called the kinetic loop, is a good indicator of the activity of the electrode [17]. The diameter of the kinetic loop is a measurement of the charge

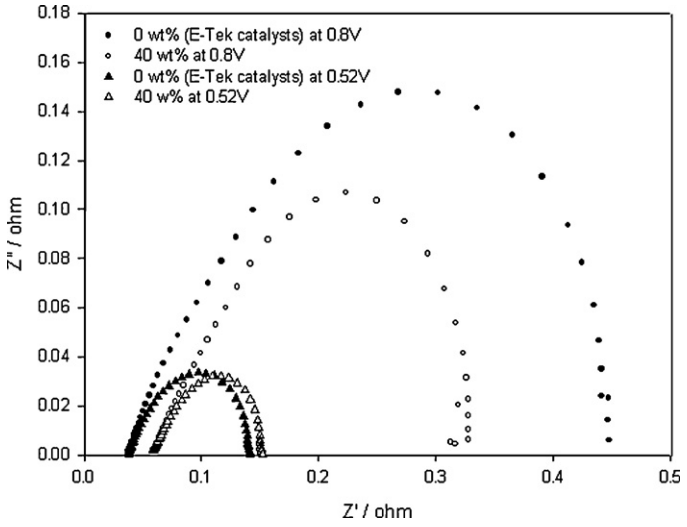

Fig. 12. Nyquist plots for the cathodic electrodes with E-TEK catalysts and 40% composite catalysts (E-TEK) at 0.8 V and 0.52 V (vs. pseudo-reference electrode). The Pt loading for anode and cathode was 0.8 mg cm^{-2}.

Table 2
Resistances of cathodes with 40 wt% composite catalyst and E-TEK catalyst.

Mass fraction of Pt–Ru/C (modified) (wt%)	Resistance (Ω)	
	Calculated from cathode polarization curves	Calculated from Nyquist plots
0	0.14	0.04
40	0.11	0.06

transfer resistance of the ORR. It was believed that the 40 wt% composite catalysts (E-TEK) had a lower charge transfer resistance than E-TEK catalysts: indicating a higher activity for the 40 wt% composite catalysts (E-TEK). Referring to the Nyquist plots in Fig. 12, the high-frequency intercept of the semicircle loop on the real axis represents the ohmic resistance from the electrode and electrolyte. These Nyquist plots in Fig. 12 show that the cathode with 40 wt% composite catalysts (E-TEK) had a higher ohmic resistance and activity than the E-TEK catalysts. However, Fig. 11 reveals that the cathode with 40 wt% composite catalysts (E-TEK) gave lower overall resistance than that with E-TEK catalysts. Table 2 summarizes the overall resistances and the ohmic resistance from the polarization curves (Fig. 11) and the Nyquist plots (Fig. 12), respectively, with the 40 wt% composite catalysts (E-TEK) and the E-TEK catalysts. The difference between the resistances from polarization curves and Nyquist plots attributes to mass transfer resistance on cathode. Apparently, the E-TEK catalyst had higher mass transfer resistance than 40 wt% composite catalyst (E-TEK).

Giorgi et al. [10] reported that diffusion layer porosity influences the cell performance as the rate of mass transport of reactant gases increases with the porosity of the diffusion layer. In this case, the increase of porosity enhances the mass transport rate, as well as the performance, at high current density. It is suggested that the decrease of resistance calculated from Eq. (1), as shown in Fig. 11, was attributable to the decrease of the mass transfer resistance in catalytic layer created by adding the optimum amount of hydrophobic Pt–Ru/C (modified). Dodecylamine is generally expected to be a barrier that should increase the ohmic resistance; however, no significant effect was shown in this case. That is probably because the mass fraction of Pt–Ru/C (modified) was only 40%. As the mass fraction of Pt–Ru/C (modified) increased to more than 60 wt%, the overall resistance increased significantly.

The stability of the functional group of dodecylamine on carbon surface is under investigation. But in a preliminary test, the polarization curve of the cell with composite catalyst (E-TEK) remained unchanged after 100 h of cell performance test and electrochemical impedance analysis.

3.4. Electrolyte resistance measurement of electrode

To investigate the electrolyte resistances of the catalytic layers with various mass fractions of Pt–Ru/C (modified), the electrode with an additional resistant layer was fabricated between the Nafion membrane and the catalytic layer of cathode [11], as shown

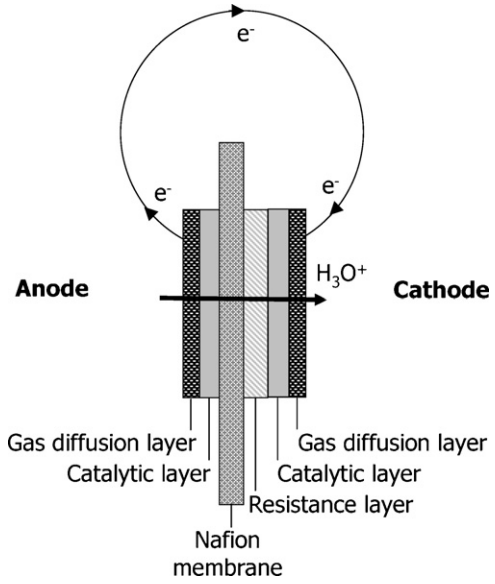

Fig. 13. Schematic diagram of the MEA with an additional resistant layer for the evaluation of electrolyte resistance.

in Fig. 13. The resistant layer comprised carbon powders and Nafion ionomer, without any Pt–Ru catalysts. This layer provided a pathway only for protons, while not allowing any electrochemical reaction to take place. The content of the Nafion ionomer in the resistant layer was the same as that in the catalytic layer. Fig. 14 shows the cell performances highlighting the effect of the resistant layers with various mass fractions of carbon (modified). Eventually, the cell performances are seen to be the same regardless of the mass fraction of carbon (modified) in the resistant layer. As the resistance layer played as a proton transport barrier between the Nafion membrane and the cathodic catalyst layer, the overall resistances with a resistant layer were higher than that without a resistance layer, as shown in Fig. 15. The resistant layers with various mass fractions of carbon (modified) revealed the same electrolyte resistance, i.e. about 0.12 Ω (the difference in the resistance with and without a resistance layer). This phenomenon indicated that the resistance of the resistance layer due to proton transport was independence of the mass fraction of carbon (modified) in the resistant layer. It

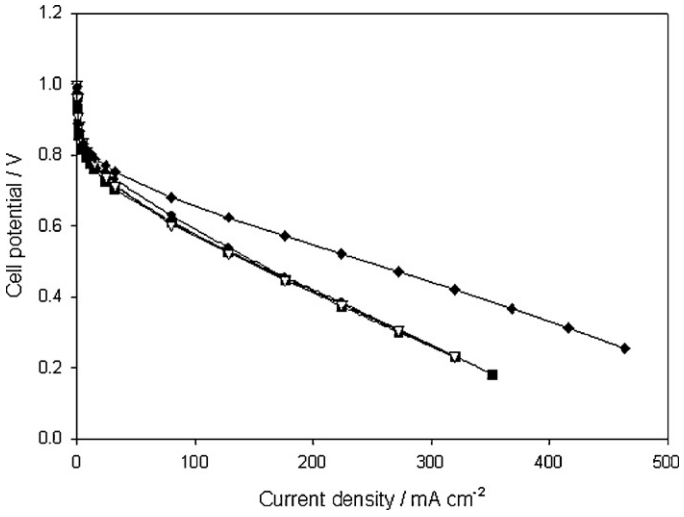

Fig. 14. Cell performances without (♦) and with resistant layers containing 0 (▼), 30 (●), 60 (▲) and 100 wt% (■) of carbon (modified). The Pt loading for anode and cathode were 0.8 mg cm^{-2}.

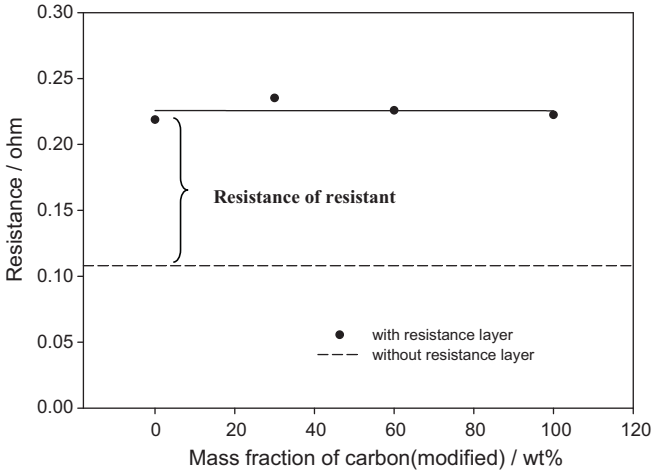

Fig. 15. Overall resistances calculated from the polarization curves as a function of the mass fraction of carbon (modified) in resistant layer.

depicted that the functional groups on the modified carbon did not affect the resistance of the resistant layer. Based on these results, it is apparent that the electrolytic resistance in the catalytic layer was independent of the mass fraction of the Pt–Ru/C (modified). The resistances of electron and gas diffusion, excluding proton transfer, were the only two resistances which were affected by the mass fraction of Pt–Ru/C (modified) in the catalytic layer.

3.5. Effect of the Pt–Ru/C (modified) catalyst in various catalyst layers

The anode and cathode performances of the MEA with various types of catalysts for the cathode were compared as shown in Fig. 16. In the low current density region, the cathodes with composite catalysts had superior performances to either E-TEK catalyst or Pt–Ru/C (raw). It is believed that the improvement in performance arose from the addition of the highly active Pt–Ru/C (modified) to the catalytic layer. At 0.5 V (vs. pseudo-reference electrode), the cathode with a composite catalyst (E-TEK) showed a current density of 373 mA cm^{-2} which was 33.7% higher than that of the E-TEK catalyst (279 mA cm^{-2}). The enhancement in the cell

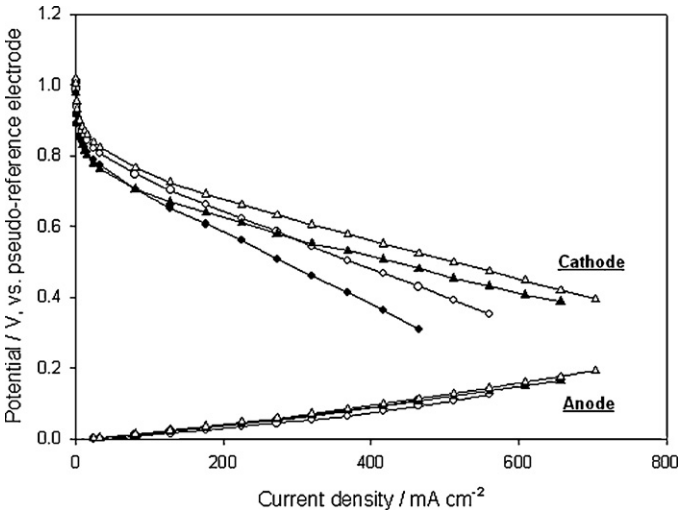

Fig. 16. Polarization curves of anode and cathode for E-TEK catalyst (●), 40 wt% composite catalyst (E-TEK) (○), Pt–Ru/C (raw) (▲) and 40 wt% composite catalyst (raw) (△) in cathode. All of the anodes used Pt–Ru/C (raw) as catalysts. The Pt loading for anode and cathode was 0.8 mg cm^{-2}.

performance also could be seen in the composite catalyst (raw) compared to the Pt–Ru/C (raw). The 40 wt% composite catalyst (raw) reached 508 mA cm^{-2} at 0.5 V (vs. pseudo-reference electrode), which is higher than Pt–Ru/C (raw) by 18.5%. It is believed that the improvement mainly arisen from the higher activity of Pt–Ru/C (modified) and the lower mass transport resistance in the catalytic layer.

4. Conclusions

This study introduced a hydrophobic catalyst with well-dispersed Pt–Ru nanoparticles on the surface of carbon supports that were first modified with dodecylamine. An improved cell performance with a maximum power density of 162 mW cm^{-2} was obtained with the cathode made of a 20–40% mass fraction of Pt–Ru/C (modified) in a composite catalyst (E-TEK). The improvement in the maximum power density by 30% arose from the lower charge transfer resistance, due to the smaller Pt–Ru nanoparticles and lower mass transport resistance. When the mass fraction of Pt–Ru/C (modified) was higher than 60%, the degrade of cell performance was mainly attributable to the increase of electron resistance resulting from the dodecylamine on the carbon surface. At the cathode potential of 0.5 V (vs. pseudo-reference electrode), the 40 wt% composite catalyst (E-TEK) gave a higher current density (373 mA cm^{-2}) than E-TEK catalyst by 33.7%. The 40 wt% composite catalyst (raw) reached 508 mA cm^{-2} at 0.5 V (vs. pseudo-reference electrode), higher than Pt–Ru/C (raw) by 18.5%.

Acknowledgments

This research was supported by the National Science Council of Taiwan, under the contract of NSC 96-2221-E-006-130. A special appreciation should go to Mr. J.C. Lee for his technical helps in XPS.

References

[1] X. Li, S. Ge, C.L. Hui, I.M. Hsing, Electrochem. Solid State Lett. 7 (2004) A286.
[2] M Chen, Y.C. Xing, Langmuir 21 (2005) 9334–9338.
[3] Y. Kim, T. Mitani, J. Catal. 238 (2006) 394–401.
[4] G. Wu, D.Y. Li, C.S. Dai, D.L. Wang, N. Li, Langmuir 24 (2008) 3566–3575.
[5] A. Fischer, J. Jindra, H. Wendt, J. Appl. Electrochem. 28 (1998) 277–282.
[6] M.S. Wilson, S. Gottesfeld, J. Appl. Electrochem. 22 (1992) 1–7.
[7] M. Uchida, Y. Aoyama, N. Eda, A. Ohta, J. Electrochem. Soc. 142 (1995) 4143–4149.
[8] M.C. Yang, C.H. Hsueh, J. Electrochem. Soc. 153 (2006) A1043–A1048.
[9] E.A. Ticianelli, C.R. Derouin, A. Redondo, S. Srinivasan, J. Electrochem. Soc. 135 (1988) 2209–2214.
[10] L. Giorgi, E. Antolini, A. Pozio, E. Passalacqua, Electrochim. Acta 43 (1998) 3675–3680.
[11] J. Lobato, M.A. Rodrigo, J.J. Linares, K. Scott, J. Power Sources 157 (2006) 284–292.
[12] J.F. Moulder, W.F. Stick, P.E. Sobol, K.D. Bomben, Handbook of X-ray Photoelectro Spectroscopy, PerkinElmer, Eden Prairie, MN, 1992.
[13] P.L. Kuo, W.F. Chen, C.Y. Lin, J. Power Sources 194 (2009) 234–242.
[14] J. Sharma, S. Mahima, A.B. Kakade, R. Pasricha, A.B. Mandale, K. Vijayamohanan, J. Phys. Chem. B 108 (2004) 13280–13286.
[15] A. Haimov, H. Cohen, R. Neumann, J. Am. Chem. Soc. 126 (2004) 11762–11763.
[16] J. Sharma, N.K. Chaki, A.B. Mandale, R. Pasricha, K.J. Vijayamohanan, Colloid Interface Sci. 272 (2004) 145–152.
[17] X.Z. Yuan, H.J. Wang, J.C. Sun, J.J. Zhang, Int. J. Hydrogen Energy 32 (2007) 4365–4380.